energies

MDPI

Article

A Novel DSP-Based MPPT Control Design for Photovoltaic Systems Using Neural Network Compensator †

Ming-Fa Tsai *, Chung-Shi Tseng, Kuo-Tung Hung and Shih-Hua Lin

Department of Electrical Engineering, Minghsin University of Science and Technology, 1, Xinxing Rd., Xinfeng, Hsinchu 30401, Taiwan; cstseng@must.edu.tw (C.-S.T.); danny.hung@chan-yue.com (K.-T.H.); ypp@must.edu.tw (S.-H.L.)

* Correspondence: mftsai@must.edu.tw; Tel.: +886-3-5593142 (ext. 3070); Fax: +886-3-5573895

† This paper is an extended version of our paper published in 2012 IEEE 21st International Symposium on Industrial Electronics, Hangzhou, China, 28–31 May 2012; pp. 1742–1747.

Abstract: In this study, based on the slope of power versus voltage, a novel maximum-power-point tracking algorithm using a neural network compensator was proposed and implemented on a TI TMS320F28335 digital signal processing chip, which can easily process the input signals conversion and the complex floating-point computation on the neural network of the proposed control scheme. Because the output power of the photovoltaic system is a function of the solar irradiation, cell temperature, and characteristics of the photovoltaic array, the analytic solution for obtaining the maximum power is difficult to obtain due to its complexity, nonlinearity, and uncertainties of parameters. The innovation of this work is to obtain the maximum power of the photovoltaic system using a neural network with the idea of transferring the maximum-power-point tracking problem into a proportional-integral current control problem despite the variation in solar irradiation, cell temperature, and the electrical load characteristics. The current controller parameters are determined via a genetic algorithm for finding the controller parameters by the minimization of a complicatedly nonlinear performance index function. The experimental result shows the output power of the photovoltaic system, which consists of the series connection of two 155-W TYN-155S5 modules, is 267.42 W at certain solar irradiation and ambient temperature. From the simulation and experimental results, the validity of the proposed controller was verified.

Keywords: maximum-power-point tracking; photovoltaic system; neural network compensator; genetic algorithm

Citation: Tsai, M.-F.; Tseng, C.-S.; Hung, K.-T.; Lin, S.-H. A Novel DSP-Based MPPT Control Design for Photovoltaic Systems Using Neural Network Compensator †. *Energies* **2021**, *14*, 3260. https://doi.org/10.3390/en14113260

Academic Editors: Marco Mussetta, Faranda Roberto Sebastiano, Hossein Hafezi and Emanuele Ogliari

Received: 14 May 2021
Accepted: 1 June 2021
Published: 2 June 2021

1. Introduction

Climate change and environmental pollution are the main issues in the world over the past two decades. The increasing depletion of fossil fuels to produce carbon is the cause of the problems. Thus, every country actively searches for renewable energy to achieve the goal of carbon neutrality. Among the renewable energies, the solar and wind energies are most popular and must be extracted by using power converters and control technology to become a stable power supply [1]. Recently, due to the ease of installation, the rapid growth in power electronics, and advanced control techniques, solar energy has become more and more popular in electric power applications [2–5]. In order to obtain the highest output efficiency of photovoltaic (PV) arrays, the techniques of the maximum power point tracking (MPPT) for solar energy conversion systems are necessary.

Many algorithms have been developed to provide maximum PV power, such as the perturbation and observation method, incremental conductance method, and hill-climbing method [6–16]. The perturbation and observation method, in which the duty cycle of the power converter is selected to be perturbed, is often used for the MPPT problem because it is easy to implement; however, an oscillation problem is inevitable [6–9]. The incremental conductance method is used to reduce oscillation by comparing the incremental

and instantaneous conductance of the PV arrays, but the implemented circuit is more complex [10–14]. The hill-climbing method, in which the voltage of the PV array is selected to be perturbed, has the advantage of omitting the current feedback circuit, but its control algorithm is more complex [15,16]. Furthermore, the control algorithm of the short-circuit pulse-based MPPT method is simple and leaves out the voltage feedback circuit, but the drift of operating point due to partially shaded effect is still an open problem [17–20].

Conventionally, the solar energy conversion systems are composed of a PV array, a dc/dc converter, a dc/ac inverter, batteries, and a center-tapped transformer. Practically, the characteristics of PV output voltage and output current are determined by the number of solar irradiation conditions, ambient temperature, and electrical load characteristics. Thereby, the technologies of changing the location of the maximum power point must be developed in the applications of MPPT control in order to make the PV array obtain the optimal efficiency from solar energy at different operating conditions. Neural networks with multi-layer neurons are widely used to approximate an arbitrary input–output mapping of an uncertain PV system [21–24]. In [24], a neural-network-based MPPT control of a PV array is worked together with an interleaved boost converter using a fuzzy controller, which may complicate the system. Recently, a low-complexity MPPT algorithm that is based on the neural network model of the photovoltaic module was proposed, but it needs three variables including solar irradiance, temperature, and voltage as the inputs to the input layer of the neural network, in which the solar irradiance is also estimated by another three-layer neural network [25].

In this study, the uncertainties of solar irradiation conditions, cell temperature, and the electrical load characteristics in PV systems are compensated by a neural network, and the duty cycle of the dc/dc converter is determined by a proportional-integral (PI) controller, the parameters of which are determined off-line by a genetic algorithm (GA) with the help of MATLAB [26,27]. The control objective is to achieve MPPT for the PV system, including a solar cell array, a dc/dc converter, and an output load despite the variation in solar irradiation, cell temperature, and the electrical load characteristics in PV systems. By the simulation of MATLAB and implementation of a DSP TMS320F28335, a prototype PV system around 310W with an MPPT controller is built in this study.

The next section describes that the PV system output power is a function of the solar irradiation, cell temperature, and characteristics of the PV array. Moreover, the analytic solution for obtaining the maximum power is difficult to obtain due to its complexity, nonlinearity, and uncertainties of parameters. The innovation of this work is to obtain the maximum power of a PV system using a neural network, in which the variables of solar irradiance and temperature are not necessary as the inputs of the neural network, with the idea of transferring the MPPT problem into a current control problem. The current controller parameters are determined via a genetic algorithm for finding the controller parameters by the minimization of a complicatedly nonlinear performance index function. In addition, it only needs the PV array output voltage and current as the inputs of the neural network, which contains only six neurons totally. From experimental results, the validity of the proposed MPPT controller was verified under certain solar irradiation and partially shaded conditions.

This paper is organized as follows: The materials for the PV system and the proposed control method are described in Section 2. The simulation verification in MATLAB/Simulink and the experimental results using a digital signal processing chip are presented in Section 3. Finally, the conclusions are in Section 4.

2. The Materials for the PV System and the Proposed Control Method

2.1. PV Array

A PV array consists of a number of series and parallel connections of PV modules, each of which consists of a number of series and parallel connections of PV cells. A PV cell is a nonlinear device, which consists of a light-generated DC current source I_{ph}, a diode D, a resistance R_{sh} shunt with this current source, and a series resistance R_s. The equivalent

circuit of the PV cell can be depicted in Figure 1, where I_{ph} is directly proportional to the solar irradiance, the parallel resistance R_{sh} illustrates the leakage current, and the series resistance R_s represents the Ohmic losses [26].

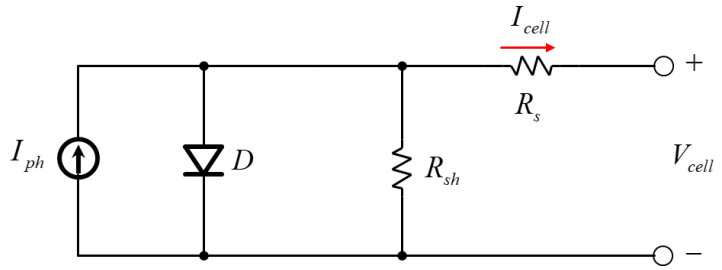

Figure 1. The equivalent circuit of a photovoltaic (PV) cell.

In general, for simplicity, R_{sh} and R_s can be neglected. The simplified mathematical model of the output current of the PV cell is given as

$$I_{cell} = I_{ph} - I_{rs}(e^{\frac{qV_{cell}}{pkT}} - 1) \tag{1}$$

where q is the electric charge, k is the Boltzmann's constant, T is the cell surface temperature (°K), p is the cell ideality factor ($p = 1 \sim 5$), and I_{rs} is the cell reverse saturation current. The mathematical model of the reverse saturation current is given as follows:

$$I_{rs} = I_{rr}(\frac{T}{T_r})^3 e^{\frac{qE_{gp}}{pk}(\frac{1}{T_r} - \frac{1}{T})} \tag{2}$$

where T_r is the reference temperature, I_{rr} is the reverse saturation current at the reference temperature, and E_{gp} is the band gap energy ($E_{gp} \approx 1.1$ eV).

Let N_p be the number of PV cells in parallel and N_s be the number of PV cells in series in a PV module. Then the output current I_{PV} of a PV module is given as

$$I_{PV} = N_p I_{ph} - N_p I_{rs}(e^{\frac{qV_{PV}}{N_s pkT}} - 1) = I_{sc} - N_p I_{rs}(e^{\frac{qV_{PV}}{N_s pkT}} - 1) \tag{3}$$

where V_{PV} is the output voltage of the PV module, I_{sc} is the short-circuit current of the PV module and expressed as

$$I_{sc} = N_p I_{ph} \tag{4}$$

While the PV module is open-circuit, the output current I_{PV} is zero. Then the cell reverse saturation current in (1) can be obtained from (3) as

$$I_{rs} = \frac{1}{N_p} \frac{I_{sc}}{e^{\frac{qV_{oc}}{N_s pkT}} - 1} \tag{5}$$

where V_{oc} is the open-circuit voltage of the PV module.

In addition, the short-circuit current of the PV module varied according to solar irradiation and cell temperature is given below:

$$I_{sc} = (I_{scr} + K_I(T - T_r))\frac{\lambda}{1000} \tag{6}$$

where I_{scr} is the short-circuit current at the reference temperature and solar radiation, K_I the short circuit current temperature coefficient at the reference temperature and solar radiation, and λ is the solar irradiance (W/m^2). The open-circuit voltage of the PV module varied according to cell temperature is given below:

$$V_{oc} = V_{ocr} + K_V(T - T_r) \tag{7}$$

where V_{ocr} is the open-circuit voltage at the reference temperature and K_V is the open-circuit voltage temperature coefficient at the reference temperature.

Furthermore, let n_p be the number of PV modules in parallel and n_s be the number of PV modules in series in the PV array of a PV system. Then the output current of the PV array is given as

$$i_{pv} = n_p I_{sc} - n_p N_p I_{rs}(e^{\frac{qv_{pv}}{n_s N_s pkT}} - 1) \tag{8}$$

The output power of PV array is expressed as follows:

$$P_{pv} = i_{pv} v_{pv} \tag{9}$$

The power versus voltage curves for different solar irradiation and temperature of a PV array with one module (TYN-155S5) are shown in Figure 2a,b, respectively. As can be seen, the output power P_{pv} is determined by the solar irradiation, cell temperature, and characteristics of a PV array. The purpose of this study is to develop an MPPT controller for the PV array to obtain its maximum power under the environment of different solar irradiation and temperature.

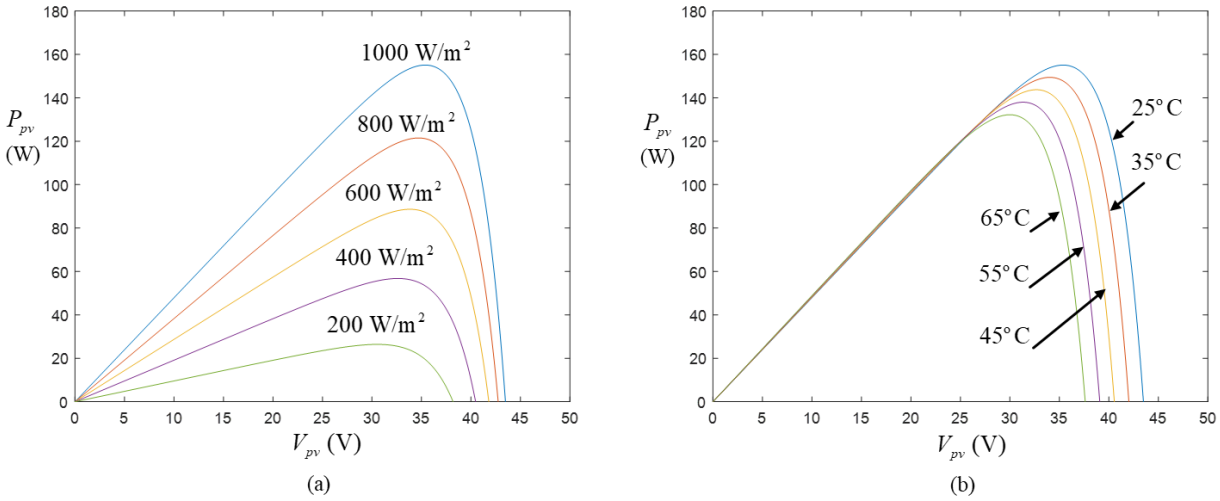

Figure 2. The power versus voltage curves: (**a**) for different solar irradiation, (**b**) for different temperature.

2.2. A Novel Control Structure for PV Array with MPPT

2.2.1. Problem Formulation of MPPT for PV System

The conventional MPPT algorithms use (10) as follows to obtain the maximum output power point.

$$\frac{\partial P_{pv}}{\partial v_{pv}} = 0 \tag{10}$$

Substituting (8) and (9) into (10) yields

$$\frac{\partial P_{pv}}{\partial v_{pv}} = i_{pv} - v_{pv} \frac{n_p N_p I_{rs} q}{n_s N_s pkT} e^{\frac{qv_{pv}}{n_s N_s pkT}} = 0 \tag{11}$$

In other words, if (11) can be achieved, then the maximum power point tracking is also followed.

As mentioned above, the output power P_{pv} is determined by solar irradiation, cell temperature, and characteristics of PV arrays, and so is the derivative with respect to v_{pv}. Moreover, the analytic solution of (11) is difficult to obtain due to its complexity and nonlinearity. This is the reason why it is so difficult to solve the MPPT problem for a PV system. Thus, a neural network is proposed to solve the problem by learning the nonlinear function and is described as follows.

By observing (11), the parameters I_{rs} (reverse saturation current), T (ambient temperature), and p (cell ideality factor) are uncertain terms. Let $T = T_0 + \Delta T$, $p = p_0 + \Delta p$, $I_{rs} = I_{rs0} + \Delta I_{rs}$, where T_0, p_0, and I_{rs0} denote nominal terms and ΔT, Δp, and ΔI_{rs} denote perturbed terms for T, p, and I_{rs}, respectively. Therefore, Equation (11) can be rewritten as follows [28]:

$$\begin{aligned} & i_{pv} - v_{pv}\frac{n_p N_p I_{rs} q}{n_s N_s pkT} e^{\frac{qv_{pv}}{n_s N_s pkT}} \\ & = i_{pv} - v_{pv}\frac{n_p N_p (I_{rs0}+\Delta I_{rs}) q}{n_s N_s (p_0+\Delta p) k (T_0+\Delta T)} e^{\frac{qv_{pv}}{n_s N_s (p_0+\Delta p) k (T_0+\Delta T)}} \\ & = i_{pv} - [v_{pv}\frac{n_p N_p I_{rs0} q}{n_s N_s p_0 k T_0} e^{\frac{qv_{pv}}{n_s N_s p_0 k T_0}} + (v_{pv}\frac{n_p N_p I_{rs} q}{n_s N_s pkT} e^{\frac{qv_{pv}}{n_s N_s pkT}} - v_{pv}\frac{n_p N_p I_{rs0} q}{n_s N_s p_0 k T_0} e^{\frac{qv_{pv}}{n_s N_s p_0 k T_0}})] \\ & = i_{pv} - (x_0 + \Delta x) \end{aligned} \tag{12}$$

where nominal term

$$x_0 = v_{pv}\frac{n_p N_p I_{rs0} q}{n_s N_s p_0 k T_0} e^{\frac{qv_{pv}}{n_s N_s p_0 k T_0}} \tag{13}$$

and perturbed term

$$\Delta x = v_{pv}\frac{n_p N_p I_{rs} q}{n_s N_s pkT} e^{\frac{qv_{pv}}{n_s N_s pkT}} - x_0 \tag{14}$$

From the above analysis, x_0 is determined by the nominal value of the PV system and Δx is function of the uncertain parameters I_{rs}, T, and p. This study proposes a novel controller for the MPPT problem to compensate the uncertainty Δx using neural networks as follows.

Define a tracking error as follows:

$$e = i_{pv} - (x_0 + \Delta \hat{x}) \tag{15}$$

where $\Delta \hat{x}$ is an estimate of uncertainty Δx and is an output of the neural network. The purpose of the proposed controller, with the structure shown in Figure 3, is to make $i_{pv} - (x_0 + \Delta \hat{x})$ approach zero, which is equivalent to achieving MPPT for the PV system. The inputs of the neural networks are i_{pv} and v_{pv}, and the weightings in the neural network are adjusted by the tracking error e, at the same time the duty cycle of the dc/dc converter is regulated by a PI controller. By observing (14), although the current i_{pv} is not relative to the uncertainty Δx, it will affect the variations in the uncertain parameters I_{rs}, T, and p. Therefore, it is also used as an input to the input layer of the neural network for increasing the learning speed.

2.2.2. The Structure of the Proposed Recurrent Neural Network

In this study, a recurrent neural network is adopted to compensate for the uncertainties in the PV system. The structure of the proposed neural network compensator is shown in Figure 4, which includes an input layer, a hidden layer, and an output layer. It only needs the PV array output current and voltage as the inputs of the neural network. Only six neurons totally are enough for the control scheme. This structure is much simpler than the existing work in [25], which needed three variables, including solar irradiance, temperature, and voltage as the inputs to the input layer of the neural network, the solar irradiance variable in which is also estimated by an additional three-layer neural network.

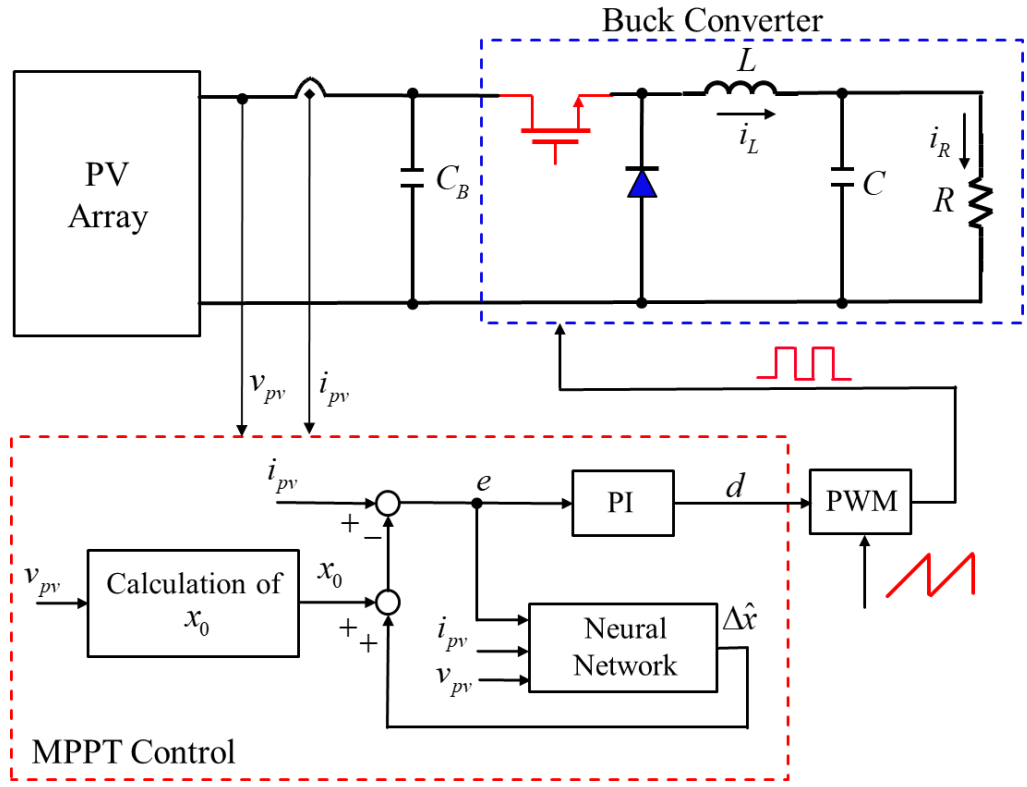

Figure 3. The structure of the proposed controller of a PV system based on a neural network.

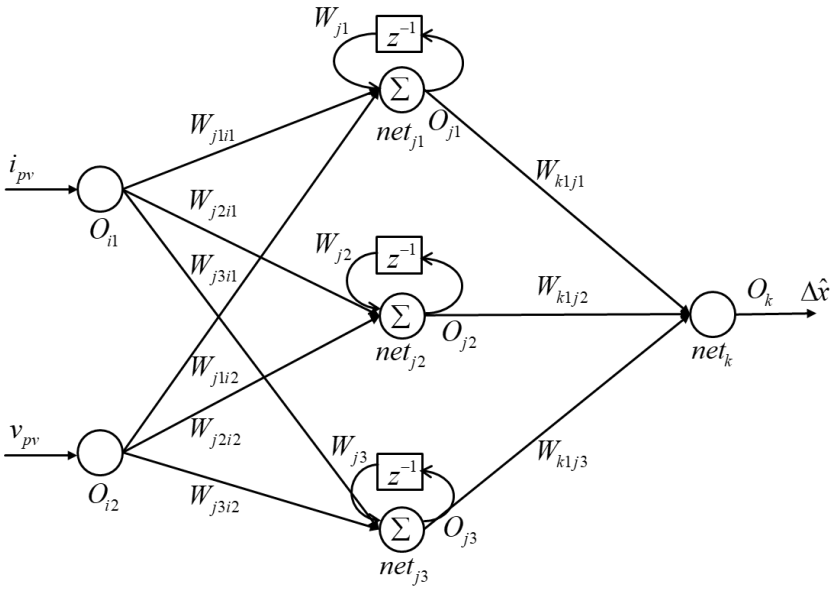

Figure 4. The structure of a recurrent neural network with two inputs i_{pv} and v_{pv}.

The structure of the employed neural network is described as follows:

- Input Layer:

There are two inputs, which are the output current i_{pv} and output voltage v_{pv} of the PV system, on the input layer. The outputs of the ith node in the input layer are defined as

$$O_i(N) = \frac{1}{1 + e^{-x_i(N)}}, i = 1, 2 \tag{16}$$

where $x_1 = i$ and $x_2 = \omega$, respectively. N denotes the iteration number.

- Hidden layer:

There are three nodes (j = 1, 2, 3) in the hidden layer for simplicity of implementation. The outputs of the jth node in the hidden layer are defined as

$$O_j(N) = \frac{1}{1 + e^{-net_j(N)}}, j = 1,\ 2,\ 3 \tag{17}$$

where

$$net_j(N) = W_j \times O_j(N-1) + \sum_i [W_{ji} \times O_i(N)] \tag{18}$$

The updating of the weights, W_j, W_{ji}, and W_{kj} are defined, respectively, as follows. Firstly,

$$W_j(N+1) = W_j(N) + \Delta W_j(N) \tag{19}$$

where

$$\Delta W_j(N) = \eta_j \delta_k W_{kj} \times P_j(N) \tag{20}$$

where δ_k is called the propagation error and given by the tracking error as

$$\delta_k = e \tag{21}$$

and

$$P_j\Big(N) = f_j'(net_j(N))[O_j(N-1) + W_j(N)P_j(N-1)] \tag{22}$$

In (22), we have

$$f_j'(net_j(N)) = \frac{\partial O_j(N)}{\partial net_j(N)} = \frac{e^{-net_j(N)}}{\left(1 + e^{-net_j(N)}\right)^2} \tag{23}$$

Secondly,

$$W_{ji}(N+1) = W_{ji}(N) + \Delta W_{ji}(N) \tag{24}$$

where

$$\Delta W_{ji}(N) = \eta_{ji} \delta_k W_{kj} \times Q_{ji}(N) \tag{25}$$

In (25), we have

$$Q_{ji}\Big(N) = f_j'(net_j(N))[O_i(N) + W_j(N)Q_{ji}(N-1)] \tag{26}$$

and

$$W_{kj}\Big(N+1) = W_{kj}(N) + \Delta W_{kj}(N) \tag{27}$$

where

$$\Delta W_{kj}(N) = \eta_{kj} \delta_k O_j(N) \tag{28}$$

In (20), (25), and (28), η_j, η_{ji}, and η_{kj} are the learning rate, respectively.

- Output Layer:

There is only one output node in the output layer (k = 1) and is defined as

$$net_k(N) = \sum_j \Big[W_{kj} \times O_j(N)\Big] \tag{29}$$

$$O_k = net_k \tag{30}$$

2.3. PI-Controller Designed by GA Algorithm

A PI current controller is to be designed by a GA algorithm to make the current control tracking error be zero. The performance index is defined as

$$J = \int_0^\infty e^2 dt \tag{31}$$

To find the optimal value of the performance index function using GA, we confine the search domain of the PI controller parameters k_p and k_i within a constraint area, which is determined as follows. Figure 5 shows the controlled plant of the current control system, in which d is the duty cycle of the PWM signal to control the switch of the buck converter. The current i_L is approximately equal to the PV output current i_{pv} and is also near equal to the load current i_R at the steady state because they are DC currents. The transfer function from the duty cycle to the output load current can be obtained as (32).

$$G_p(s) = \frac{I_R(s)}{D(s)} = \frac{v_{pv}}{RLCs^2 + Ls + R} \tag{32}$$

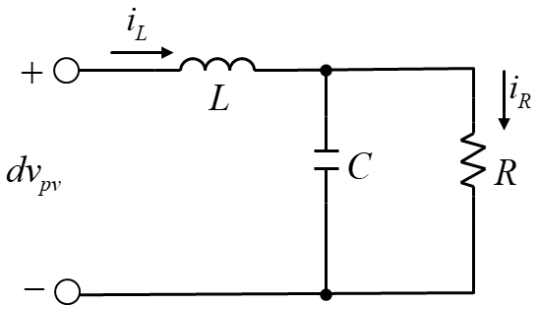

Figure 5. The controlled plant of the current controller.

The transfer function block diagram of the PV current control system using the PI controller is shown in Figure 6. It can be derived that the closed-loop transfer function is

$$G_{cl}(s) = \frac{D(s)}{I_R^*(s)} = \frac{(k_p s + k_i)(RLCs^2 + Ls + R)}{RLCs^3 + Ls^2 + (R + k_p v_{pv})s + k_i v_{pv}} \tag{33}$$

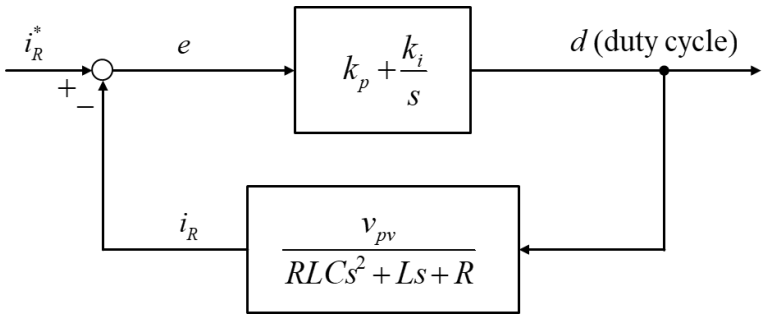

Figure 6. The transfer function block diagram of the PV current control system.

Thus, for a unit-step current reference, the Laplace transform of the duty cycle can be expressed as

$$D(s) = \frac{1}{s} \frac{(k_p s + k_i)(RLCs^2 + Ls + R)}{RLCs^3 + Ls^2 + (R + k_p v_{pv})s + k_i v_{pv}} \tag{34}$$

By using initial value theorem, the initial value of the duty cycle can be written as

$$d(0^+) = \lim_{s\to\infty} sD(s) = \lim_{s\to\infty} \frac{(k_p s + k_i)(RLCs^2 + Ls + R)}{RLCs^3 + Ls^2 + (R + k_p v_{pv})s + k_i v_{pv}} = k_p \tag{35}$$

Because the duty cycle must be between zero and one ($0 \leq d(t) \leq 1$), it follows that

$$0 \leq k_p \leq 1 \tag{36}$$

The limit of the parameter k_i can be obtained by using the Routh–Hurwitz criterion. Consider that the characteristic equation of the closed-loop system in (33) is of the form

$$RLCs^3 + Ls^2 + (R + k_p v_{pv})s + k_i v_{pv} = 0 \tag{37}$$

Table 1 shows the Routh's tabulation to determine the stability of the system. For the system to be stable, the criterion indicates that

$$k_i > 0 \tag{38}$$

and

$$L(R + k_p v_{pv}) - RLCk_i v_{pv} > 0 \tag{39}$$

which are on the first column of the Routh's tabulation and must be positive as the other elements of the column. It turns out from (39) that

$$k_i < \frac{L(R + k_p v_{pv})}{RLCv_{pv}} \tag{40}$$

Table 1. The Routh's tabulation.

	Column 1	**Column 2**
s^3	RLC	$R + k_p v_{pv}$
s^2	L	$k_i v_{pv}$
s^1	$\frac{L(R+k_p v_{pv})-RLCk_i v_{pv}}{L}$	0
s^0	$k_i v_{pv}$	

For finding the k_p and k_i parameters of the PI controller by minimizing the performance index in (31), the calculation of the performance index has to be also obtained and is described as follows.

From Figure 6, the transfer function from the current reference to the tracking error is

$$\frac{E(s)}{I_R^*(s)} = \frac{1}{1 + (k_p + \frac{k_i}{s})\frac{v_{pv}}{(RLCs^2+Ls+R)}} = \frac{s(RLCs^2 + Ls + R)}{RLCs^3 + Ls^2 + (R + k_p v_{pv})s + k_i v_{pv}} \tag{41}$$

Thus, for a unit-step current reference ($I_R^*(s) = 1/s$), the Laplace transform of the tracking error can be expressed as

$$E(s) = \frac{RLCs^2 + Ls + R}{RLCs^3 + Ls^2 + (R + k_p v_{pv})s + k_i v_{pv}} = \frac{b_2 s^2 + b_1 s + b_0}{a_3 s^3 + a_2 s^2 + a_1 s + a_0} \tag{42}$$

where $a_3 = b_2 = RLC$, $a_2 = b_1 = L$, $a_1 = R + k_p v_{pv}$, $a_0 = k_i v_{pv}$, $b_0 = R$. Then, using Parseval's theorem, the performance index can be rewritten as

$$\begin{aligned} J &= \int_0^\infty e^2 dt = \frac{1}{2\pi j}\int_{-j\infty}^{j\infty} [E(-s)E(s)]ds \\ &= \frac{b_2^2 a_0 a_1 + (b_1^2 - 2b_0 b_2)a_0 a_3 + b_0^2 a_2 a_3}{2a_0 a_3(-a_0 a_3 + a_1 a_2)} \end{aligned} \tag{43}$$

Because it is very difficult to determine the PI controller's parameters k_p and k_i by the minimization of the performance index in (43), which is a complicatedly nonlinear function, this problem can be solved by using GA with the help of the MATLAB simulation tool. After the constraints of the PI controller's parameters and the calculation of the performance index are obtained, the program code of the cost function in MATLAB based on (36), (38), (39), and (43) is illustrated in Figure 7. This function file is called by the main program of the GA algorithm via a "degademo" function, which is shipped with MATLAB. By setting the maximum number of generations to be 200, mutation rate equal to 0.15, crossover rate equal to 0.7, similarity limit equal to 10^{-8} in the main program, the performance index curve convergence behavior, with respect to the generations, is shown in Figure 8. As can be seen, it is convergent to the steady value of 3.1688×10^{-4} on the twentieth generation. Executing the MATLAB main program file also reports the optimal values of the PI controller parameters, which are:

$$k_p = 0.9967 \tag{44}$$

and

$$k_i = 125.4710 \tag{45}$$

```
function f = GApvcost(xyData)
global R L C Vpv
[Nxy,Mxy]=size(xyData);   % Nxy length of population
for i=1:Nxy
     Kp  =  xyData(i,1);
     Ki  =  xyData(i,2);
     a3 = R*L*C;
     a2 = L;
     a1 = R+Vpv*Kp;
     b2 = a3;
     b1 = a2;
     b0 = R;
     if (a2*a1-a0*a3>0 && Kp<1 && Ki>0 && Kp>0)     %error term
        z1=-(b2^(2)*a0*a1+(b1^(2)-
             2*b0*b2)*a0*a3+b0^(2)*a2*a3)/(2*a0*a3*(-a0*a3+a1*a2));
        z(i)=z1;
     else
        z(i)=-10000; % %if Ki<0 or a2*a1-a0*a3<0 then escape this
%improper set of parameters (put a very large cost in this case).
     end
end
f = z'; %cost output
%degademo is a function of Matlab.
%degademo finds maximal value of the cost function.
%Hence, we put a minus sign in front of our cost to find a minimal cost
%by using degademo.
%(a2*a1-a0*a3>0)is the stability condition from Routh-Hurwitz table.
```

Figure 7. The MATLAB function called by degademo.m file.

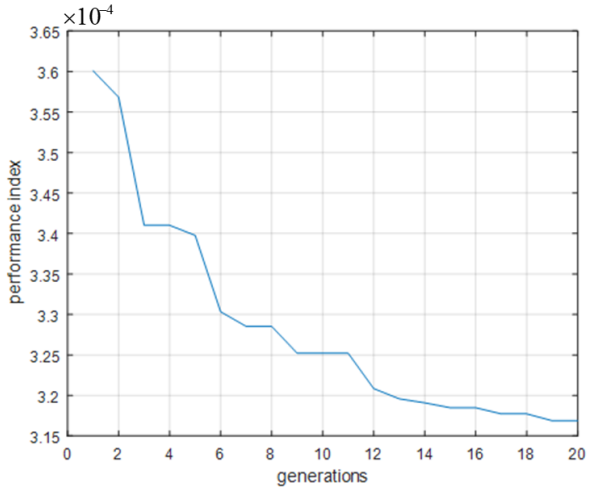

Figure 8. The performance index curve with respect to generations.

The step responses of the load current i_R and the inductor current i_L in the closed-loop system using the designed PI controller's parameters via GA are shown in Figure 9a,b, respectively. As can be seen, the inductor current response is smoother than the load current in the transient state, and both achieve the steady-state value without error.

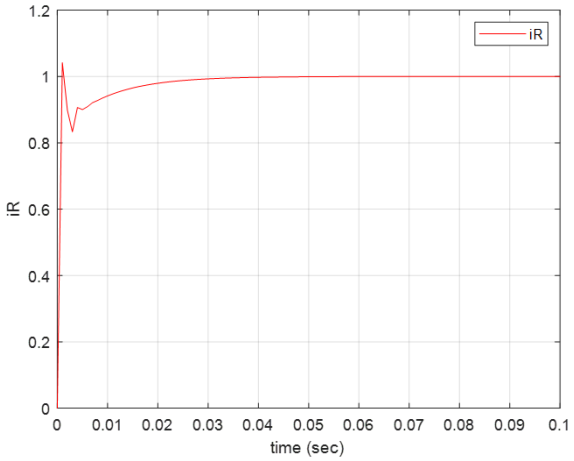

(**a**)

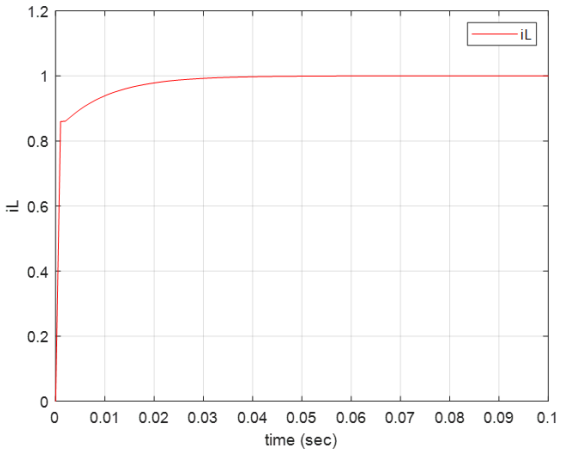

(**b**)

Figure 9. The step response using the designed PI controller: (**a**) load current, (**b**) inductor current.

3. Results and Discussion

3.1. Model Verification

Before the simulation analysis of the proposed MPPT control scheme of the PV system, the model of the PV array, which is composed of one or more PV modules, with the parameters shown in Table 2, was constructed and verified. The PV array model with the PV modules series and parallel connection for the case of $n_s = 2$, $n_p = 1$ and the case of $n_s = 2$, $n_p = 2$, was constructed, respectively, as shown in Figure 10a,b, in which the PV module block using the embedded MATLAB function was built based on Equations (1)–(8) in the previous section with $n_p = N_p = n_s = 1$ and $N_s = 64$, as shown in Figure 11. The output of the PV module function was then used to control a current source for the generation of the output current of the PV module. In the first case, the load resistance was given as 15.8 $\Omega(= 70.02/4.43)$ for obtaining the maximum power of the PV array. As indicated in Figure 10a, the output power, current, and voltage values were displayed with the power value of 309.9 W, which is near the maximum power of 310 W, and the current and voltage value at 4.428 A and 69.99 V, respectively.

Table 2. The PV module parameters (TYN-155S5) (@1 kW/m^2, 25 °C).

Electrical Characteristics	Specification
Maximum Power (Pmax)	155 W
Current at Maximum Power (Imp)	4.43 A
Voltage at Maximum Power (Vmp)	35.01 V
Short-Circuit Current	4.79 A
Open-Circuit Voltage	43.49 V
Short-Circuit Current Temperature Coefficient (K_I)	2.5 mA/°C
Open-Circuit Voltage Temperature Coefficient (K_V)	−0.147 V/°C

In the second case, the load resistance was given as 7.9 $\Omega(= 70.02/8.86)$ for obtaining the maximum power of the PV array. As indicated in Figure 10b, the output power, current, and voltage values were displayed with the power value of 619.8 W, which is near the maximum power of 620 W and is the double value of the first case, and the current and voltage value at 8.856 A and 69.99 V, respectively. The results of both cases verify the validation of the PV array model, which can be extended to a larger PV array easily by setting the series connection number n_s and the parallel connection number n_p of the PV module.

3.2. Simulation Verification

To illustrate the effectiveness of the proposed controller, a PV array of 310 W composed of two cascaded solar panels, a buck converter, a PI controller, a neural network, and an output load was also constructed. The simulation block diagram of the proposed MPPT controller for the PV system with the buck converter switching frequency of 10 kHz and neural network updating rate of 100 Hz using MATLAB/Simulink is shown in Figure 12. The neural network compensator has one input for the tracking error for tuning the weighting in the hidden layer, two input nodes (i = 1, 2) for the two input variables i_{pv} and v_{pv}, three hidden nodes (j = 1, 2, 3), and one output node (k = 1) for the $\Delta\hat{x}$.

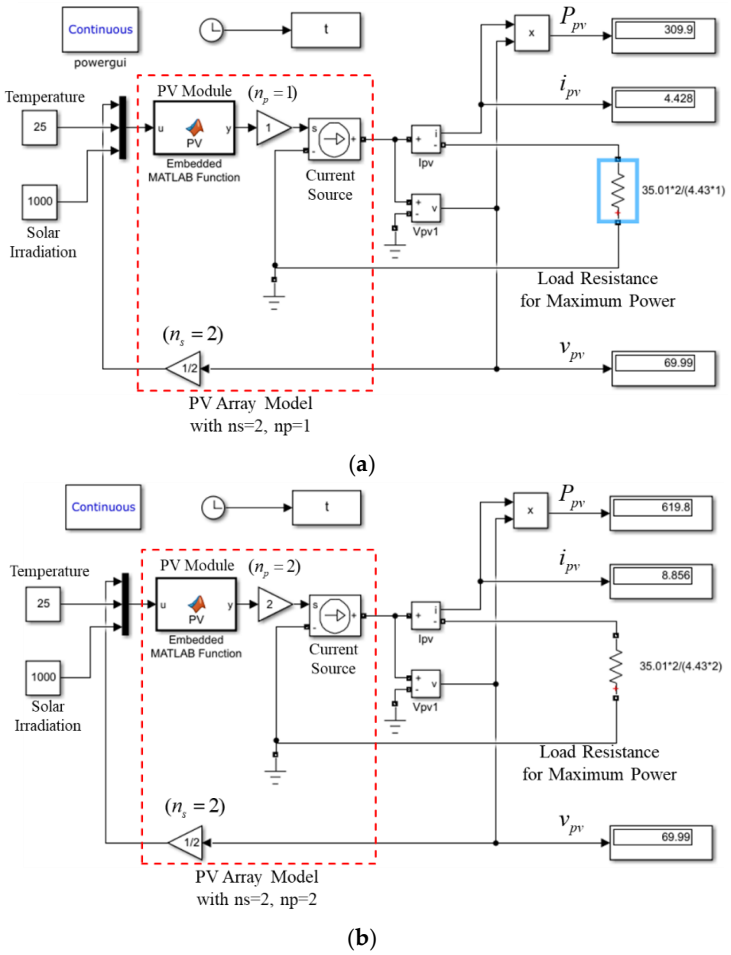

Figure 10. PV array model construction and verification: (**a**) with $n_s = 2$, $n_p = 1$, (**b**) with $n_s = 2$, $n_p = 2$.

```
function y = PV(u)
Vpv=u(1);   % PV module output voltage
T=u(2)+273; % cell temperture
Lumda=u(3); % solar irradiation
Ns=64;      % series connection of the cell in the PV module
p=2;        % cell identity factor
n=Ns*p;
k=1.38e-23; % Boltzmann constant
q=1.6e-19;
Iscr=4.79;  % shirt-circuit current
Vocr=43.49; % open-circuit voltage
Tr=298;
ki=2.5e-3;  % shirt-circuit current temperature coefficient
kv=-0.147;  % open-circuit voltage temperature coefficient
Ior=Iscr/(exp(q/n/k/Tr*Vocr)-1);
Isc=(Iscr+ki*(T-Tr))*Lumda/1000;
Vocr1=((n*k*Tr)/q)*log((Ior+Isc)/Ior);
Voc=(Vocr1+kv*(T-Tr));
Irr=Isc/(exp(q/n/k/T*Voc)-1);
Io=Irr*T*T*T/Tr/Tr/Tr*exp(q*1.1/p/k*(1/Tr-1/T));
Id=Io*(exp(q/n/k/T*Vpv)-1);
y=Isc-Id;
```

Figure 11. THe PV module function.

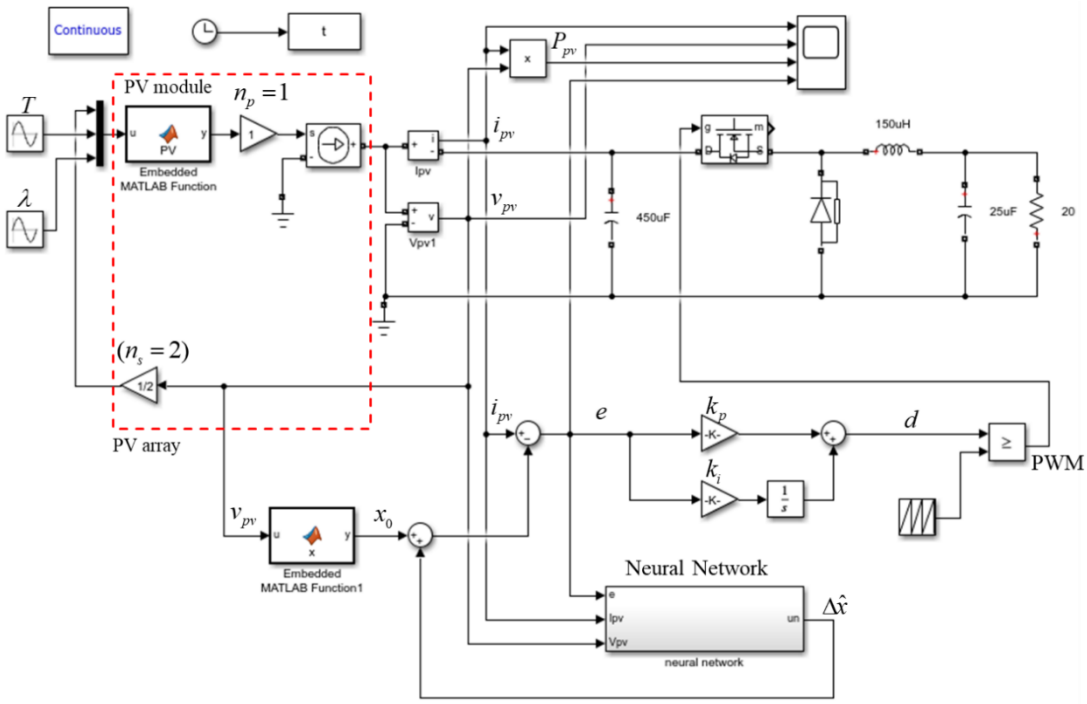

(**a**)

```
function y = x(u)
% The function for x0
p=2;          % cell identity factor
Ns=64;
n=Ns*p;
Np=1;
ns=2;
np=1;
k=1.38e-23;
q=1.6e-19;
T0=298;       % norminal temperature
Isc0=4.79;    % nominal short-circuit current
Voc0=43.49; % nominal open-circuit voltage
Irs0=Isc0/[exp(q/n/k/T0*Voc0)-1];
a=q*Irs0*np*Np/(ns*n*k*T0);
b=a*exp(q*u/(ns*n*k*T0));
y=b*u;
```

(**b**)

Figure 12. The simulation block construction: (**a**) PV system model, (**b**) nominal function for x_0.

The PI controller parameters designed by GA were then used on the simulation model of the 310-W PV system, in which the embedded MATLAB function for x_0 based on (13) in the previous section is shown in Figure 12b, for the overall simulation verification of the proposed MPPT control performance. Figure 13 shows the simulated results for the sudden changes in solar irradiation from 200 W/m^2 up to 1000 W/m^2 with a change of 200 W/m^2 at each time step of 0.1 s at the ambient temperature of 25 °C. As can be seen, the output current, voltage, and the power of the PV array can quickly reach the steady-state value of each step, and the output power can reach the maximum value of 310 W with the current valve at about 4.4 A and the voltage value at about 70.0 V while the solar irradiation increases up to 1000 W/m^2. In addition, the tracking error is approaching zero despite the sudden changes in solar irradiation. This is equivalent to achieving MPPT for the PV system.

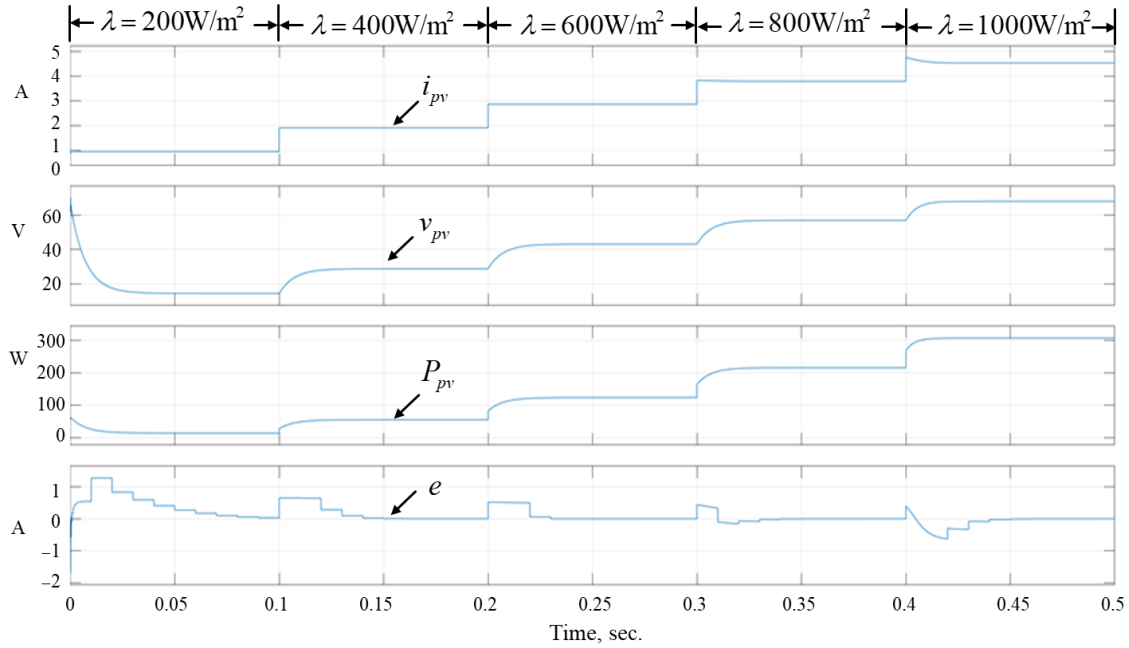

Figure 13. Simulation results for the sudden changes in the solar irradiation.

The next simulation is for the condition of continuous variations in the ambient temperature at the solar irradiation of 1000 W/m^2 as follows: $T = T_0 + \Delta T$, $T_0 = 25$ °C, $\Delta T = 40 \sin \omega t$ (°C), $\omega = 5$ rad/s. The simulated results are shown in Figure 14. As can be seen in Figure 14a, the PV array's output current, voltage, and hence the output power are varied due to the variations in the ambient temperature. The output power of the PV array can also reach the maximum value of about 310 W. The corresponding MPPT control signals of the tracking error e, neural network output $\Delta\hat{x}$, the nominal value x_0, and the sum of x_0 and $\Delta\hat{x}$ are also shown in Figure 14b. As can be seen, the signal of the sum of x_0 and $\Delta\hat{x}$ can track the output current of the PV array very well, so that the tracking error is convergent to be zero despite the variation in ambient temperature.

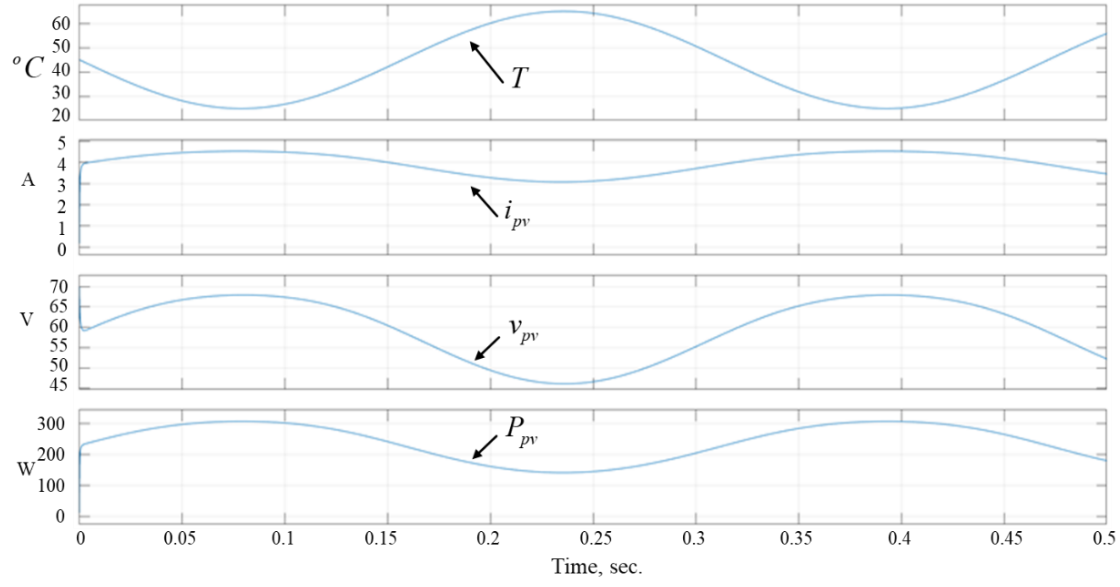

(**a**)

Figure 14. *Cont.*

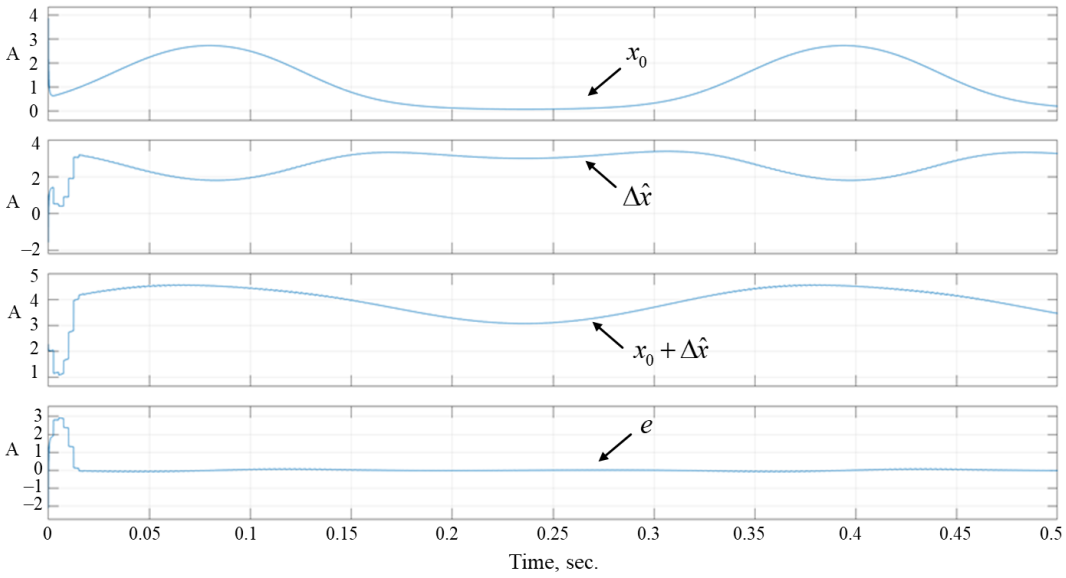

(**b**)

Figure 14. Simulation results for the variations in the ambient temperature: (**a**) the signals of temperature, output current, voltage, and power, (**b**) the MPPT control signals.

3.3. DSP Implementation and Experimental Verification

In this study, the proposed controller was implemented by a TI TMS320F28335 DSP chip embedded on an eZdsp control board, which can easily process the input signals conversion and the complex floating-point computation on the neural network of the proposed control scheme. Figure 15 shows the basic configuration of the PV system. The PV output current is detected by using a LEM LA-55P current sensor followed by two-stage operational amplifiers for the conversion and low-pass filtering as a voltage signal. The PV output voltage is also detected by using a difference amplifier. The two signals are then read by the DSP chip through a multi-channel 12-bit built-in A/D converter. The signals of the MPPT control can be viewed either on the Code Composer of the DSP development software system or on the oscilloscope by using a 12-bit SPI-DAC converter with output voltage scaled in the range from 0 to 5 V outside the DSP control board. The training data of the neural network inputs i_{pv} and v_{pv} are sampled from the A/D converters in every 0.01 s on line to compute the output $\Delta\hat{x}$. Comprehensive experiments are made to investigate the proposed MPPT capability for the PV system.

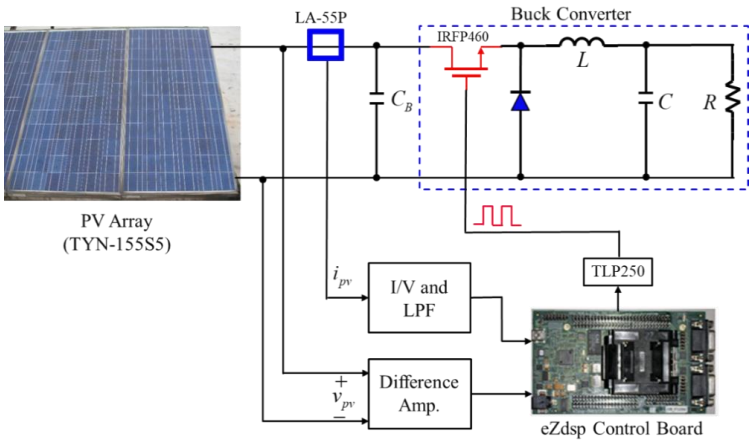

Figure 15. The basic configuration of the PV system.

At certain solar irradiation and ambient temperature, output waveforms of the proposed MPPT controller for the PV array, which consists of the series connection of two 155-W TYN-155S5 PV modules, are shown in Figure 16, and the experimental data at the final steady-state is shown in Table 3. The result indicates the output current, voltage, and power of the PV array are from lower values increasing up to the maximum values of 4.14 A, 64.53 V, and 267.42 W, respectively, at that solar irradiation and ambient temperature condition.

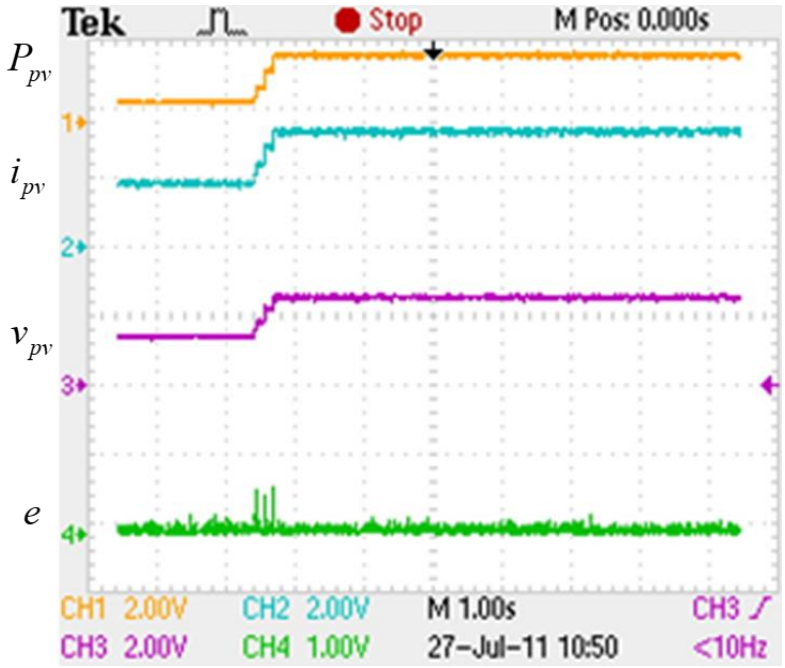

Figure 16. The output waveforms of the PV system at a certain solar irradiation.

Table 3. The experimental data of Figure 16 at steady-state on the view of Code Composer.

Name	Value	Type	Radix
i_{pv}	4.143993	float	float
v_{pv}	64.53333	float	float
P_{pv}	267.4218	float	float
e	0.01850748	float	float

To illustrate the effectiveness of the proposed MPPT controller under partially shaded conditions, the PV array is covered by a board and removed after a while. The output waveforms of this case are shown in Figure 17. From the experimental result, the proposed controller can make the tracking error approach zero under partially shaded conditions despite the variation in solar irradiation, ambient temperature, and the electrical load characteristics in the PV system, which is equivalent to achieving MPPT for the PV array under partially shaded conditions.

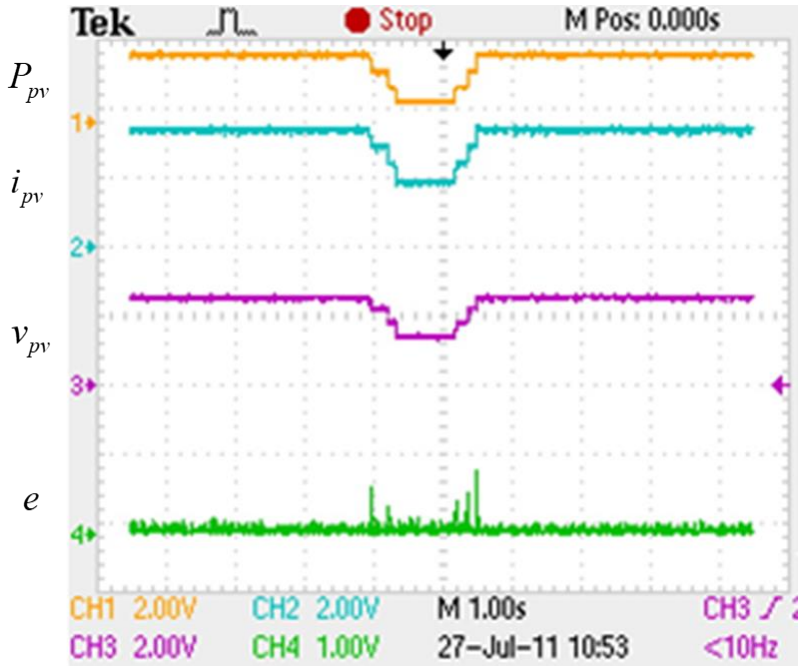

Figure 17. Output waveforms of PV array covered by a board and then removed.

4. Conclusions

In this study, based on the slope of power versus voltage, a novel MPPT algorithm using a neural network compensator was proposed and implemented on a TI TMS320F28335 DSP chip, which can easily process the input signals conversion and the complex floating-point computation on the neural network of the proposed control scheme. It was derived that the output power of the photovoltaic system is a function of the solar irradiation, cell temperature, and characteristics of the photovoltaic array. The analytic solution for obtaining the maximum power is difficult to obtain due to its complexity, nonlinearity, and uncertainties of parameters. Therefore, the MPPT control scheme is presented to solve the abovementioned problems using neural network with the idea of transferring the MPPT problem into a current PI control problem. In addition, the neural network system, which contains six neurons totally, only needs the PV array output voltage and current as the inputs of the input layer and the tracking error signal for updating the weighting of the neurons in the hidden layer. This structure is simpler than the existing work, which needs three variables as the inputs to the input layer of the neural network.

The current PI controller's parameters are to be determined by minimizing a performance index function, which is the time integral of the square of the tracking error signal of the current controller from zero infinity and can be transformed into a nonlinear function containing the controller parameters by Parseval's theorem. Because it is very difficult to determine the PI controller's parameters by the minimization of the complicatedly nonlinear function, this problem can be solved by using GA with the help of the MATLAB simulation tool. A function file that lists the nonlinear performance index function and the constraints of the PI controller parameters determined by the initial-value theorem and Routh–Hurwitz criterion for the stability check, respectively, is called by the main program of the GA algorithm via a "degademo" function. The performance index curve is convergent to the steady value of a very small value on the twentieth generation by executing the main program, which also reports the optimal values of the PI controller parameters.

The model of the PV array, which is composed of two PV modules in a series connection, was constructed and used for the simulation verification of the proposed MPPT control scheme. The PV model can be extended to a larger array easily by setting the series and the parallel connection numbers of the PV module.

The experimental result shows the output current, voltage, and power of the PV array are increasing up to the maximum values of 4.14 A, 64.53 V, and 267.42 W, respectively, at the solar irradiation and ambient temperature condition. The proposed controller can also make the tracking error approach zero, which is equivalent to achieving MPPT for the PV array under partially shaded conditions.

The proposed control scheme can be applied to the MPPT-based solar chargers and PV inverters. More experiments will be conducted in the near future to compare with the available products in the market, such as Fronius Symo 15.0-3-M. The maximum efficiency for PV grid of this inverter is 98.1%, with MPP adaptation efficiency greater than 99.9%, in which two MPP trackers (MPPT 1 and MPPT 2) are installed so as to connect PV arrays with different solar azimuth and tilt angles, with different string lengths, and connect strings of dissimilar modules. The presented control scheme might be better than the dual-tracker scheme because it can obtain the maximum power despite the variation in solar irradiation, cell temperature, the effect of uncertain parameters, and the electrical load characteristics in the PV systems.

Author Contributions: Conceptualization, C.-S.T.; Data curation, K.-T.H.; Formal analysis, M.-F.T.; Funding acquisition, C.-S.T.; Investigation, M.-F.T.; Methodology, M.-F.T.; Project administration, C.-S.T.; Resources, M.-F.T., K.-T.H. and S.-H.L.; Software, K.-T.H.; Supervision, C.-S.T.; Validation, K.-T.H.; Visualization, M.-F.T. and C.-S.T.; Writing—original draft, M.-F.T. and C.-S.T.; Writing—review & editing, M.-F.T. All authors have read and agreed to the published version of the manuscript.

Funding: This research was funded by Project number: NSC 100-2221-E-159-008 from the Ministry of Science and Technology (MOST), Taiwan.

Acknowledgments: This work was supported by the Ministry of Science and Technology of Taiwan under Contract NSC 100-2221-E-159-008.

Conflicts of Interest: The authors declare no conflict of interest.

References

1. Tsai, M.-F.; Tseng, C.-S.; Lin, B.-Y. Phase voltage-oriented control of a PMSG wind generator for unity power factor correction. *Energies* **2020**, *13*, 5693. [CrossRef]
2. Ahmed, J.; Salam, Z. An accurate method for MPPT to detect the partial shading occurrence in a PV system. *IEEE Trans. Ind. Inform.* **2017**, *13*, 2151–2161. [CrossRef]
3. Pei, T.; Hao, X.; Gu, Q. A novel global maximum power point tracking strategy based on modified flower pollination algorithm for photovoltaic systems under non-uniform irradiation and temperature conditions. *Energies* **2018**, *11*, 2708. [CrossRef]
4. Ahmad, R.; Murtaza, A.F.; Sher, H.A. Power tracking techniques for efficient operation of photovoltaic array in solar applications—A review. Renewable Sustain. *Energy Rev.* **2019**, *101*, 82–102.
5. Lam, L.; Phuc, T.; Hieu, N. Simulation models for three-phase grid connected PV inverters enabling current limitation under unbalanced faults. *Eng. Technol. Appl. Sci. Res.* **2020**, *10*, 5396–5401. [CrossRef]
6. Bendib, B.; Belmili, H.; Krim, F. A survey of the most used MPPT methods: Conventional and advanced algorithms applied for photovoltaic systems. *Renew. Sustain. Energies Rev.* **2015**, *45*, 637–648. [CrossRef]
7. Alik, R.; Jusoh, A. Modified Perturb and Observe (P&O) with checking algorithm under various solar irradiation. *Sol. Energy* **2017**, *148*, 128–139.
8. Bradai, R.; Boukenoui, R.; Kheldoun, A.; Salhi, H.; Ghanes, M. Experimental assessment of new fast MPPT algorithm for PV systems under nonuniform irradiance conditions. *Appl. Energy* **2017**, *199*, 416–429. [CrossRef]
9. Andrean, V.; Chang, P.-C.; Lian, K.-L. A review and new problems discovery of four simple decentralized maximum power point tracking algorithms—Perturb and observe, incremental conductance, golden section search, and newton's quadratic interpolation. *Energies* **2018**, *11*, 2966. [CrossRef]
10. Chen, Y.; Lai, Z.; Liang, R. A novel auto-scaling variable step-size MPPT method for a PV system. *Sol. Energy* **2014**, *102*, 247–256. [CrossRef]
11. Faraji, R.; Rouholamini, A.; Naji, H.R.; Fadaeinedjad, R.; Chavoshian, M.R. FPGA-based real time incremental conductance maximum power point tracking controller for photovoltaic systems. *IET Power Electron.* **2014**, *7*, 1294–1304. [CrossRef]
12. Tey, K.S.; Mekhilef, S. Modified incremental conductance MPPT algorithm to mitigate inaccurate responses under fast-changing solar irradiation level. *Sol. Energy* **2014**, *101*, 333–342. [CrossRef]
13. Elgendy, M.A.; Zahawi, B.; Atkinson, D.J. Assessment of the incremental conductance maximum power point tracking algorithm. *IEEE Trans. Sustain. Energy* **2013**, *4*, 108–117. [CrossRef]

14. Li, C.; Chen, Y.; Zhou, D.; Liu, J.; Jun Zeng, J. A high-performance adaptive incremental conductance MPPT algorithm for photovoltaic systems. *Energies* **2016**, *9*, 288. [CrossRef]
15. Piegari, L.; Rizzo, R.; Spina, I.; Tricoli, P. Optimized adaptive perturb and observe maximum power point tracking control for photovoltaic generation. *Energies* **2015**, *8*, 3418–3436. [CrossRef]
16. Petrone, G.; Spagnuolo, G.; Teodorescu, R.; Veerachary, M.; Vitelli, M. Reliability issues in photovoltaic power processing systems. *IEEE Trans. Ind. Electron.* **2008**, *55*, 2569–2580. [CrossRef]
17. Noguchi, T.; Togashi, S.; Naltamoto, R. Short-circuit pulse-based maximum-power-point tracking method for multiple photovoltaic-and-converter module system. *IEEE Trans. Ind. Electron.* **2002**, *49*, 217–223. [CrossRef]
18. Patel, H.; Agrwal, V. Maximum power point tracking scheme for PV systems operating under partially shaded conditions. *IEEE Trans. Ind. Electron.* **2008**, *55*, 1689–1698. [CrossRef]
19. Windarko, N.A.; Habibi, M.N.; Sumantri, B.; Prasetyono, E.; Efendi, M.Z. A new MPPT algorithm for photovoltaic power Generation under uniform and partial shading conditions. *Energies* **2021**, *14*, 483. [CrossRef]
20. Shams, I.; Mekhilef, D.S.; Soon, T.K. Maximum power point tracking using modified butterfly optimization algorithm for partial shading, uniform shading and fast varying load conditions. *IEEE Trans. Power Electron.* **2021**, *36*, 5569–5581. [CrossRef]
21. Veerachary, M.; Senjyu, T.; Uezato, K. Neural-network-based maximum-power-point tracking of coupled-inductor interleaved-boost-converter-supplied PV system using fuzzy controller. *IEEE Trans. Ind. Electron.* **2003**, *50*, 749–758. [CrossRef]
22. Taherbaneh, M.; Faez, K. Maximum power point estimation for photovoltaic systems using neural networks. In Proceeding of the IEEE Int. Conf. on Control and Automation, Guangzhou, China, 30 May–1 June 2007; pp. 1614–1619.
23. Lin, W.-M.; Hong, C.-M.; Chen, C.-H. Neural network based MPPT control of stand-alone hybrid power generation system. *IEEE Trans. Power Electron.* **2011**, *26*, 3571–3582. [CrossRef]
24. Elobaid, L.M.; Abdelsalam, A.K.; Zakzouk, E.E. Artificial neural network-based photovoltaic maximum power point tracking techniques: A survey. *IET Renew. Power Gener.* **2015**, *9*, 1043–1063. [CrossRef]
25. Zečević, Ž.; Rolevski, M. Neural network approach to MPPT control and irradiance estimation. *Appl. Sci.* **2020**, *10*, 5051. [CrossRef]
26. Jang, J.-S.R.; Sun, C.-T.; Mizutani, E. *Neuro-Fuzzy and Soft Computing*; Prentice Hall: Hoboken, NJ, USA, 1997.
27. Jang, J.-S.R.; Galley, N. *MATLAB Fuzzy Logic Toolbox User's Guide*; MathWorks Inc.: Natick, MA, USA, 1997.
28. Tsai, M.-F.; Tseng, C.-S.; Hong, G.-D.; Lin, S.-H. A Novel MPPT Control Design for PV Modules Using Neural Network Compensator. In Proceedings of the 2012 IEEE 21st International Symposium on Industrial Electronics, Hangzhou, China, 28–31 May 2012; pp. 1742–1747.